Solar Energy 204 (2020) 635–643

Contents lists available at ScienceDirect

Solar Energy

journal homepage: www.elsevier.com/locate/solener

Study on the solar energy absorption of hybrid solar cells with trapezoid-pyramidal structure based PEDOT:PSS/c-Ge

Fei Zhao[a,b], Xifang Chen[a,b], Zao Yi[a,b,*], Feng Qin[a,b], Yongjian Tang[a,b], Weitang Yao[a,b], Zigang Zhou[a,b], Yougen Yi[c]

[a] Joint Laboratory for Extreme Conditions Matter Properties, Southwest University of Science and Technology, Mianyang 621010, China
[b] Sichuan Civil-Military Integration Institute, Mianyang 621010, China
[c] College of Physics and Electronics, Central South University, Changsha 410083, China

ARTICLE INFO

Keywords:
Solar cells
Solar energy absorption
PEDOT:PSS
Pyramid
FDTD

ABSTRACT

In this paper, we have utilized finite difference time domain (FDTD) method to investigate the solar energy absorption of hybrid solar cells (HSCs) with trapezoid-pyramidal structure (TPs) based PEDOT:PSS/c-Ge. We have changed some parameters of TPs (different heights and different ratios of top to bottom) to study its effects on the solar energy absorption for HSCs. The optimization of geometric parameters is based on the maximum solar energy absorption efficiency. The optical absorption of the HSCs with TPs is basically above 90% from ~300 nm to ~1300 nm and the average solar energy absorption is 93.8% under AM 1.5 solar spectrum (from 300 nm to 1500 nm). Simultaneously, we have calculated the short-circuit current density (J_{sc}), open-circuit voltage (V_{oc}), fill factor (FF), maximum power (P_{max}) and photoelectric conversion efficiency (PCE) respectively through DEVICE software. The results of electrical simulation reveal that the maximum J_{sc} is 43.47 mA/cm^2, it is 45.73% higher than planar PEDOT:PSS/c-Ge HSCs. Moreover, to further explain the mechanism of solar energy absorption of HSCs with TPs, the logarithmic figures of electric field intensity for trapezoid-pyramidal PEDOT:PSS/c-Ge HSCs and planar PEDOT:PSS/c-Ge HSCs at different wavelengths are analyzed. The result shows that TPs array has shown excellent light-trapping effect. This work reveals the huge potential of c-Ge HSCs in solar absorption, and at the same time has certain guiding significance for the structural design of Ge SCs. It is believed that through further exploration, the conversion efficiency of c-Ge HSCs will be further improved.

1. Introduction

In recent years, with the development of society, energy and environmental issues have attracted much more attention. People pay more and more attention to research clean and renewable energy, such as wind energy, geothermal energy, tidal energy, etc. (Orrego et al., 2017; Sun et al., 2018; Zhang et al., 2020). However, due to the infinite energy provided by the sun, the photovoltaic devices which can directly convert solar energy into electricity have caused extensive research (Yi et al., 2019; Wu et al., 2020; Gao et al., 2019). As we know, researchers have been working to improve the efficiency of solar cells (SCs) (Li et al., 2019; Iman et al., 2020; Van der Heide et al., 2009). The photoactive layer realizes the conversion from light energy to electricity by absorbing photons to excite electrons from the valence band to the conduction band, and then separates the generated electron-hole pairs through a PN junction to form photocurrent. The more light energy is absorbed, the more electron-hole pairs are generated, the larger the photocurrent is generated, and the efficiency of the SCs will be improved accordingly (Li et al., 2019). In order to improve the light absorption efficiency, various microstructures are fabricated on the active layer to improve the solar energy absorption (Liu et al., 2017). In recent years, various plasmon and diffractive structures have been reported, such as nanoholes, nanocones, nanopyramids, nanowires, nanorods, nanopillars, etc. (Yan et al., 2017; Qin et al., 2020; Li et al., 2020a, 2020b; Liu et al., 2019, 2018, 2020a, 2020b; Hao et al., 2019; Pan et al., 2020; Cheng and Du, 2019; Qin et al., 2020; Yu et al., 2019). Compared with nanowires and nanopores, nanopyramids are considered to be more suitable for photovoltaic applications due to its smaller surface recombination, which greatly improves the photocurrent and the photoelectric conversion efficiency of SCs (Shi et al., 2014; Liu et al., 2020c; Cheng et al., 2018). In addition, the nanopyramids exhibits excellent optical coupling and anti-reflection effects due to the gradient effect of refractive index from the top to the bottom of the pyramids (Liu et al., 2020b). Currently, crystalline silicon (c-Si) is

* Corresponding author at: Joint Laboratory for Extreme Conditions Matter Properties, Southwest University of Science and Technology, Mianyang 621010, China.
E-mail address: yizaomy@swust.edu.cn (Z. Yi).

https://doi.org/10.1016/j.solener.2020.05.030
Received 25 February 2020; Received in revised form 11 May 2020; Accepted 11 May 2020

the main candidate for second-generation thin-film solar cells. Due to the low absorption coefficient of crystalline silicon, the optical absorption of a SCs can only be increased by increasing the thickness of the crystalline silicon layer, but the material consumption and production cost of thin film SCs will be increased (Liu et al., 2020b). Simultaneously, the traditional PN junction process is accompanied by a series of high-temperature processes, such as thermal diffusion and thermal annealing after ion implantation, which greatly increases energy consumption (Wei et al., 2013). However, the combination of organic materials and crystalline silicon is conducive to breaking this process limitation (Ikeda et al., 2016). The Si/organic hybrid SCs have many merits, such as excellent mechanical properties, simple manufacturing processes, low temperature processing and low cost (Zhang et al., 2016). Recently, a high performance organic-nanostructured silicon HSC has been reported with an efficiency as high as 14.08% (Duan et al., 2018). Besides, different nanostructures have been reported based on organic–inorganic HSCs (Ren et al., 2016; Huang et al., 2019). The simulation of perovskite/c-Ge SCs have also been reported (Kim et al., 2019; Wang et al., 2019). The low-cost organic HSCs have shown great potential. Poly (3,4-ethylenedioxythiophene):poly (styrenesulfonate) (PEDOT:PSS) is an ideal organic compound for photovoltaic application due to its good ductility and high transparency. Besides, it can effectively transport the holes to electrode and easy to prepare.

At present, the active layer of HSCs is made of crystalline silicon, GaAs, perovskite and organics, germanium, etc. (Dikshit et al., 2019; He et al., 2020; Yang et al., 2015; Wang et al., 2020a; Zhang et al., 2018). In multi-junction SCs, because of the narrow band gap (0.67 eV) of Ge materials, Ge is mainly used as a substrate and bottom cell to widen the absorption band (Baran et al., 2020). Moreover, it is imperative to achieve higher conversion efficiency of SCs and thinner active layers to improve the economic competitiveness (Taguchi et al., 2013). Due to the high absorption coefficient of germanium, simultaneously, the combination with organics like PEDOT:PSS help to further improve the absorption coefficient. So we can use less material to achieve higher conversion efficiency (Liu et al., 2020b). And the heterojunction of Ge helps to improve the shortcomings of single junction Ge SCs (Jia et al., 2017) Therefore, Ge is regarded as an efficient photovoltaic semiconductor material (Alcañiz et al., 2019). It has been reported that the conversion efficiency of the heterojunction Ge SCs under the AM 1.5 spectrum is 7.61% (Nakano and Shiratani, 2019). But, the c-Ge hybrid SCs with different geometric patterns are rarely studied. To this end, we have took the pyramid-like pattern (trapezoidal pyramids) on the active layer to improve solar energy absorption efficiency and carefully investigated the effect of different geometric parameters for trapezoid-pyramidal PEDOT:PSS/c-Ge HSCs.

In our research work, we chose crystalline germanium (c-Ge) as the active layer and designed a hybrid SCs with a trapezoidal pyramids structure based PEDOT:PSS/c-Ge. We have utilized finite difference time domain (FDTD) method to perform the optical simulation for HSCs. The optical absorption curves of trapezoid-pyramidal PEDOT:PSS/c-Ge HSCs and planar PEDOT:PSS/c-Ge HSCs were plotted respectively. And the optical absorption curves of HSCs with TPs at different heights and different ratios of top to bottom were further gained. Simultaneously, the electrical simulation under different geometric parameters of TPs was performed by DEVICE software. And the J_{sc}, V_{oc}, FF, P_{max} and PCE of HSCs with different geometric parameters were obtained. Besides, the figures of electric field intensity for trapezoid-pyramidal PEDOT:PSS/c-Ge HSCs and planar PEDOT:PSS/c-Ge HSCs at different wavelengths are characterized.

2. Structure and methods

There are many numerical methods to calculate and analyze the characteristics of the electromagnetic field, such as finite element boundary integration method and frequency-domain integral equation method (Liu et al., 2018; Lv et al., 2020; Qi et al., 2020). However, FDTD method is the most extensively used and efficient method of electromagnetic field analysis for SCs (Przybylski and Patela, 2019). FDTD method discretizes the Maxwell's equations in time and space domain. FDTD utilizes leapfrog algorithm to alternately calculate the electric field and magnetic fields in space domain, and the variation of electromagnetic field is imitated by the update in time domain to achieve the goal of compute. At the condition of without free charge and conducting current, for non-magnetic materials, Maxwell's equations can be expressed in the following form:

$$\frac{\partial \vec{D}}{\partial t} = \nabla \times \vec{H} \tag{1}$$

$$\vec{D}(\omega) = \varepsilon_0 \varepsilon_r(\omega)\vec{E}(\omega) \tag{2}$$

$$\frac{\partial \vec{H}}{\partial t} = -\frac{1}{\mu_0}\nabla \times \vec{E} \tag{3}$$

where $\vec{H}$, $\vec{E}$, and $\vec{D}$ are the magnetic, electric, and displacement fields respectively, while $\varepsilon_r(\omega)$ is the complex relative dielectric constant ($\varepsilon_r(\omega) = n^2$, where n is the refractive index), ε_0 is vacuum dielectric constant, μ_0 is the vacuum permeability, ω is the frequency of the electromagnetic wave. Before the optical simulation, we need to define the type of material in a specific geometric area. The purpose is to import the relationship between the complex refractive index and the frequency of the material. The simulation area is divided into many "small volumes", when the electromagnetic wave passes, the distribution of electromagnetic field and complex Poynting vector inside the model can be calculated. The software will automatically normalize the results to the situation under the AM 1.5 spectral condition, and the electromagnetic field data obtained through the monitor can calculate the transmission and reflection of the solar cell, so that the absorption spectrum can be calculated by the script. The optical power absorbed per unit volume can be expressed as:

$$P_{abs} = -\frac{\omega}{2}|\vec{E}|^2 Im\{\varepsilon\} \tag{4}$$

where $Im\{\varepsilon\}$ is the imaginary part of the permittivity, the P_{abs} is easy to calculate in FDTD simulation. The number of photons absorbed in a unit volume can be expressed as:

$$2\pi\hbar\omega \tag{5}$$

where $\hbar$ is reduced Planck constant, $2\pi\hbar\omega$ represents the single photon energy at the corresponding frequency. The integral of G in the whole range is the total light generation rate, it is a function related to space and frequency. The generation rate data will be imported into the DEVICE for electrical simulation later. Assuming that an absorbed photon generates an electron-hole pair, the electron-hole pair will be generated at the position where the photon is absorbed. Electrical simulation uses Poisson's equation and drift–diffusion equation to simulate the carrier collection by the electrode in the semiconductor. The DEVICE software can read the short-circuit current data on the electrode. By adding a scan voltage with a fixed step within a certain range to the electrode, and using a script, you can obtain a J-V curve and a P-V curve to calculate the efficiency of the solar cell. When the coverage of surface electrodes and various recombination effects are taken into account, the simulation results of the solar cells will be closer to the true value. The recombination types considered in this simulation of the proposed solar cell are Trap-assisted recombination, Auger recombination, Radiative recombination and Surface recombination.

The structure of HSCs we used is shown in Fig. 1(a). The bottom is a silver layer which acts as an electrode. The Ge substrate is overlaped on the silver layer to acts as the major active layer. The trapezoid-pyramidal array of Ge is on the Ge substrate and serves as a major region of solar energy absorption, which effectively improves the photoelectric conversion ability of the HSCs. The organic layer (PEDOT:PSS) that a P-

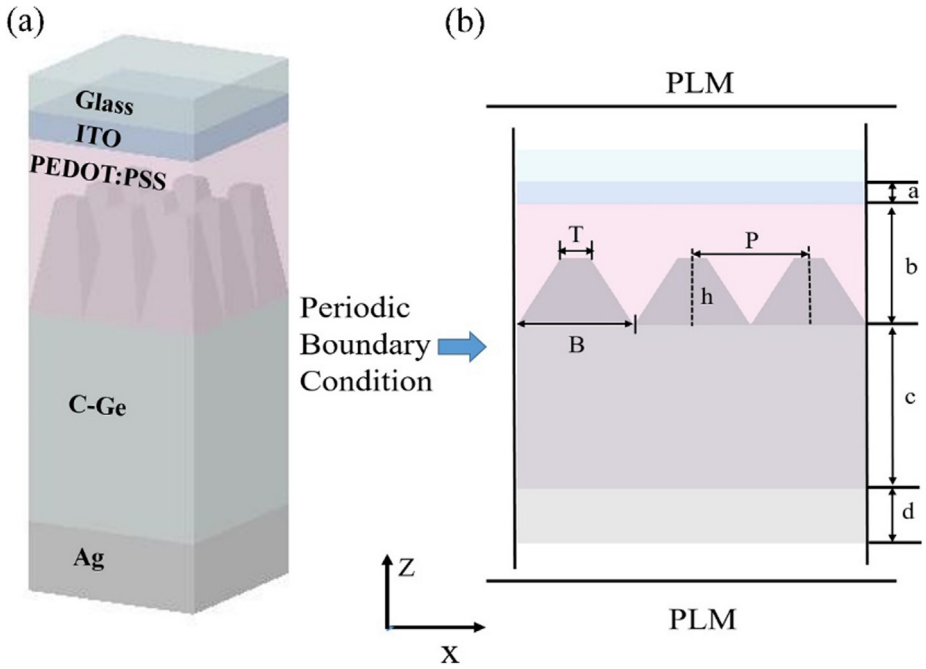

Fig. 1. The schematic of the PEDOT:PSS/c-Ge HSCs: (a) three-dimensional structure and (b) sectional view (The coordinate axis represents the direction of the sectional view).

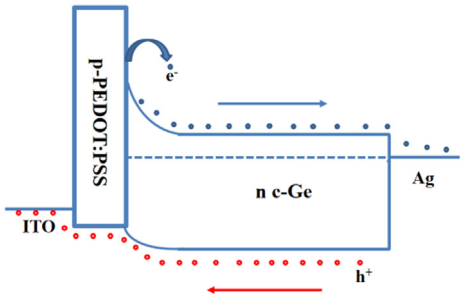

Fig. 2. Energy band diagram of carrier transport under light.

type organic material transport layer is conformally overlaped on the trapezoid-pyramidal array which is beneficial for holes to transport and can effectively prevent the electrons from passing through. Therefore, the organic layer (PEDOT:PSS) plays an important role as a hole transport layer (HTL). The transparent conductive film (ITO) is on the organic layer, which is beneficial for holes to transport and collect. Besides, we placed glass (SiO_2) on the top to gather the solar spectrum. The cross-sectional view is shown in Fig. 1(b), From top to bottom, a, b, c and d represent the thickness of ITO, PEDOT:PSS, Ge and Ag respectively, the parameters are set as: a = 80 nm, b = 500 nm, c = 600 nm, d = 200 nm. The h represents the height of the TPs, the T represents the length of the top side of the TPs, the B represents the length of the bottom side of the TPs, the P represents the period of TPs. The parameters of h, T, B and P are set as: h = 300 nm, T = 20 nm, B = 80 nm, P = 80 nm. Above geometric parameters are based on the optimization of FDTD software. Energy band diagram of carrier transport under light is shown in Fig. 2, Ge substrate is N-type doped in electrical simulation, So the Fermi level of Ge is near the bottom of the conduction band. n-type Ge and p-type PEDOT:PSS combine to form a PN junction. Therefore, the electrons are blocked by PEDOT:PSS and transmitted to the silver electrode. Because PEDOT:PSS is a good hole transport layer, So The holes are effectively transmitted through PEDOT:PSS and collected by ITO.

At the stage of the optical simulation, we have used a plane wave source with the wavelength ranged from 300 nm to 1500 nm. The HSCs is illuminated from the top and along the negative direction of the Z-axis. we used the periodic boundary condition along the direction of the X-axis and Y-axis. Along the Z-axis direction, we used the Perfectly Matched Layer (PLM) boundary conditions to avoid parasitic reflection and absorption (Niu et al., 2018). Frequency domain power monitors are used to collect the data of reflectance(R) and transmission(T) which related to the wavelength. The absorption(A) is calculated by the expression: A = 1-R-T (Wang et al., 2020b, 2020c; Huan et al., 2020; Li et al., 2020c). J_{sc} is an important parameter to describe the solar energy absorption of the SCs. It was calculated under the AM 1.5 solar spectrum condition (Wu et al., 2020). Assuming one absorbed photon generate one electron-hole pair; We can calculate the ideal short-circuit current density by the following formula:

$$J_{sc} = \frac{e}{2\pi\hbar c}\int_{300nm}^{1500nm} \lambda Q_E(\lambda) I_{AM1.5}(\lambda) d\lambda \tag{6}$$

where e is the charge on an electron, c is the speed of light, λ is the wavelength of optical source, $Q_E(\lambda)$ is the quantum efficiency of SCs and the $I_{AM1.5}(\lambda)$ is irradiance of optical source under the AM 1.5 solar spectral condition. The optical generation rate is calculated by the FDTD software and then input into the DEVICE software to calculate the electrical characteristics of the HSCs, such as V_{oc}, J_{sc}, FF, P_{max} and PCE. However, because the energy band of the crystalline semiconductors is different from the organic semiconductors. And the charge solver in DEVICE cannot calculate the electrical transport characteristics of the organic transport layer. So, the PEDOT:PSS is removed from electrical simulation. To reduce the losses and other recombination of carrier at the interface of electrode, the region which contact the electrode are highly doped. The script used in our simulation can refer to the lumerical knowledge base (Lumerical Support, n.d.).

3. Simulation result and discussion

In this study, we have investigated the optical characteristic of planar and trapezoid-pyramidal PEDOT:PSS/c-Ge HSCs. We have computed the reflection (R), transmission (T) and absorption (A) spectrum of two structure. The relationship between them is characterized by the expression: A = 1-R-T. We labeled the two structures

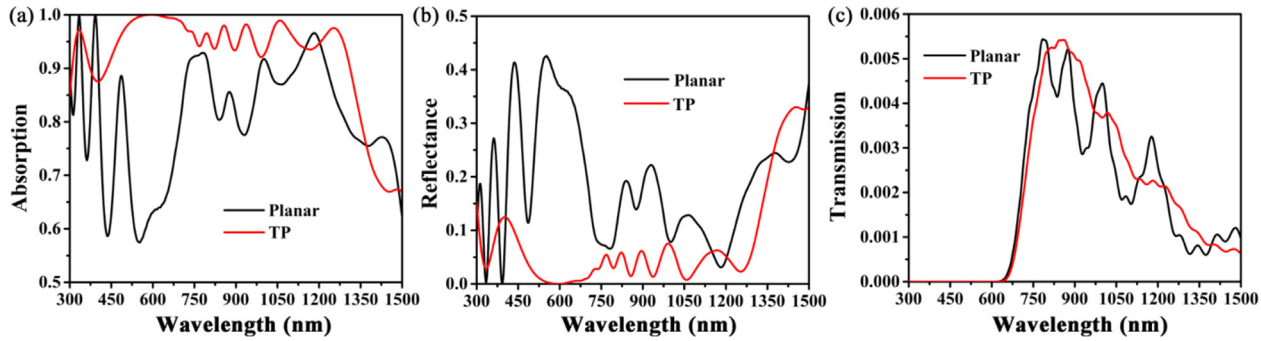

Fig. 3. (a) Absorption (b) reflectance (c) transmission spectrum of the HSCs with and without the TPs (The height of the TPs is fixed 300 nm, the length of top and bottom side are fixed 20 nm and 80 nm respectively.).

as "planar" and "TP" in Fig. 3. From Fig. 3(a), we can see that the optical absorption of the "TP" is basically above 90% from 300 nm to 1300 nm while the optical absorption of "planar" is basically below 90%, and the absorption of "TP" looks steadier than the "planar". The tapered surface of TPs drastically suppresses the reflectance due to the graded refractivity from PEDOT:PSS to c-Ge as shown in Fig. 3(b). Because the value of transmission is very small due to the reflect of Ag, the transmission has hardly any effect on the absorption. In contrast, we can find that the reflectance is a more critical parameter for optical absorption from Fig. 3(c). For example, the optical absorption of planar is relatively small at about 500 nm because of the reflectance is kind of high at 500 nm.

To further study the response of this optimized HSCs in sunlight, the absorption efficiency of trapezoid-pyramidal PEDOT:PSS/c-Ge HSCs and planar PEDOT:PSS/c-Ge HSCs are compared under the AM 1.5 solar spectrum, the results are shown in Fig. 4. As we can see from Fig. 4(a), the average absorption of planar can reach 79.44% within the whole region (300–1500 nm). The absorption performance is relatively good from 300 nm to 500 nm, while the absorption performance is degenerate a lot compared to the solar spectrum at AM 1.5. As shown in Fig. 4(b), the average absorption of trapezoid-pyramidal PEDOT:PSS/c-Ge HSCs has even reached 93.8% within the whole region (300–1500 nm). The absorption is basically coincident to the solar spectrum at AM 1.5 except the wavelength ranged from ~900 nm to ~1100 nm. Obviously, the solar energy absorption has a great improvement from trapezoid-pyramidal PEDOT:PSS/c-Ge HSCs to planar PEDOT:PSS/c-Ge HSCs.

Firstly, to further clarify the relationship between optical absorption and different geometric parameters of TPs. We have investigated the different ratios of top to bottom of the TPs. The length of bottom side and height of TPs are fixed 80 nm and 300 nm (only change the value of the length of the top side), the T^2/B^2 represents the ratios of top to bottom of the TPs (T^2/B^2 = 1/16, 1/4, 9/16 and 1/1 respectively). As shown in Fig. 5(a), it is obvious to find that the smaller the ratio of area, the smaller the maximum optical absorption. The optical coupling is enhanced by the tapered structure due to the variation of optical density. Besides, the trend of the four curves are basically coincident except the some region of black curve at about 1430 nm. There are some continuous fluctuation from the 750 nm to 1350 nm, and with the decrease of top area, the amplitude of fluctuation is compressed and the peak of wave just move right slightly except the black curve due to the difference of geometry. Moreover, the optical absorption of four curve are relatively small at about 400 nm because of the high reflectance in this region (as shown in Fig. 3(b)). In addition, we have also studied the optical absorption of HSCs with different heights of TPs. The length of bottom and top side of TPs are fixed 80 nm and 20 nm respectively (only changed the value of the height). The heights of TPs are set as 100 nm, 200 nm, and 300 nm respectively. As shown in Fig. 5(b), we can find that the blue curve and the red curve are almost coincident at the whole wave range, the red curve is slightly higher than the blue curve from 825 nm to 1350 nm. Besides, the black curve has similar trend to the other curve from 800 nm to 1500 nm. However, it is kind of different from 375 nm to 825 nm and its amplitude of fluctuation is larger than the other two. Moreover, the three curves show almost coincident in short-wave band (300 nm-380 nm). In general, the height of the trapezoidal pyramids has not big effect on the light absorption of HSCs.

We have plotted the logarithmic figure of trapezoid-pyramidal PEDOT:PSS/c-Ge HSCs and planar PEDOT:PSS/c-Ge HSCs at different wavelength. (a)–(f) in Fig. 6 show the electric field intensity distribution of trapezoid-pyramidal PEDOT:PSS/c-Ge HSCs and planar PEDOT:PSS/c-Ge HSCs at the wavelengths of 320 nm, 600 nm and 1300 nm

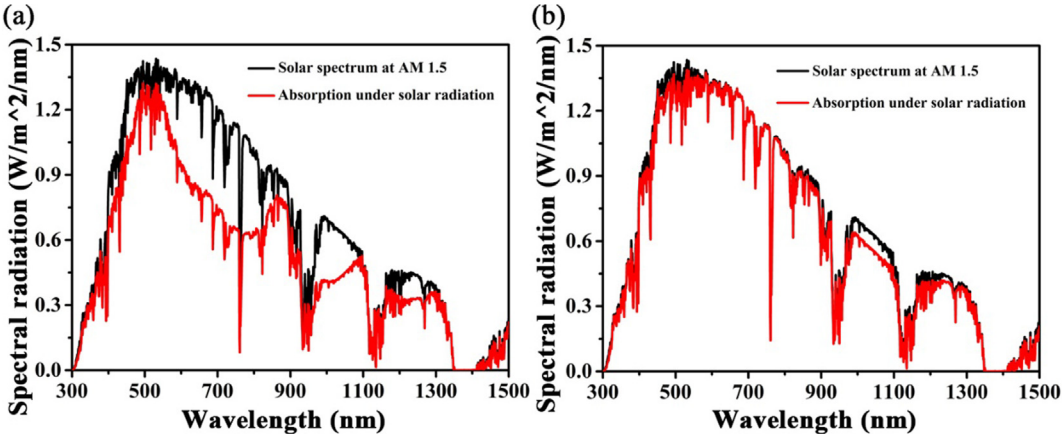

Fig. 4. (a) and (b) is the absorption spectrum of the planar PEDOT:PSS/c-Ge HSCs and trapezoid-pyramidal PEDOT:PSS/c-Ge HSCs respectively under the solar spectrum at AM 1.5.

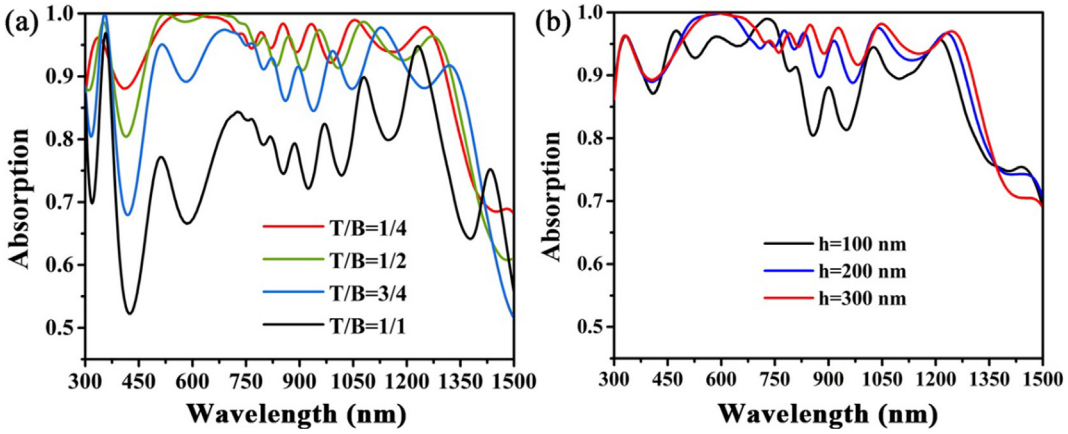

Fig. 5. (a) The spectral absorption for HSCs with different ratios of top to bottom (T^2/B^2) of the TPs (The length of bottom side and height of TPs are fixed 80 nm and 300 nm). (b) The spectral absorption of HSCs with different heights of TPs (The length of top and bottom side of TPs are fixed 20 nm and 80 nm respectively.).

respectively. As shown in Fig. 6(a, d), λ = 320 nm, for the planar PEDOT:PSS/c-Ge HSCs, the most of electric field is restricted in the organic layer and the diffraction distribution of electric field are occurred (Zhang et al., 2020; Liu et al., 2019; Wu et al., 2020). The high electric field is not exist in the Ge substrate, it is demonstrate that the most energy of short-wave is restricted in organic layer. For the trapezoid-pyramidal PEDOT:PSS/c-Ge HSCs, the higher electric field distribute uniformly in the area above the top of the TPs. The highest electric field distribute on double side of the trapezoid-pyramidal tips. In the middle region between two TPs, the electric field is decreasing gradually. It is indicated that the energy of short-wave has still not spread to the bottom between two TPs. As shown in Fig. 6(b, e), λ = 600 nm, for the planar PEDOT:PSS/c-Ge HSCs, the circumstance is similar to Fig. 6(a) while the diffractive stripes width is widened. Besides, the electric field is strengthened at the top area of Ge substrate. For the trapezoid-pyramidal PEDOT:PSS/c-Ge HSCs, the high electric field extensively distributes on the double side area of TPs. Compare Fig. 6(e) with (d), the electric field intensity of Fig. 6(e) is enhanced a lot and the area of high electric field is widened a lot too. Besides, the electric field is spread into the inside of TPs. It is consistent to the result of high absorption in Fig. 2(a) at 600 nm. The high electric field can result in the increase of optical absorption and electron-hole pairs due to the photo-coupling (Abdelraouf and Allam, 2016; Zhou et al., 2020). As shown in Fig. 6(c, f), λ = 1300 nm, for the planar PEDOT:PSS/c-Ge HSCs, with the increase of wavelength, the stripes width of diffraction is further widened on the basis of Fig. 6(b), and the additional stripes of diffraction has occurred in partial Ge substrate. It is indicated that the energy of long-wave is spread down to the Ge substrate, but not cover the whole region of Ge. For the trapezoid-pyramidal PEDOT:PSS/c-Ge HSCs, it is observed that with the red shift of the wavelength, the high electric field moves towards the bottom of the TPs, and the additional stripes of diffraction has also occurred throughout the Ge substrate. In a word, the trapezoidal pyramids structure shows a regulatory effect on optical coupling and a very good light-trapping effect to gathering the solar energy.

In order to better demonstrate the performance characteristics of the HSCs, we have selected the different geometric parameter from optical simulation and then performed electrical simulation by DEVICE software. As shown in Fig. 7(a), the V_{oc} of the "Planar" is 0.12 V and the J_{sc} is 23.59 mA/cm^2. The "TP" exhibit a V_{oc} of 0.26 V and a J_{sc} of 43.47 mA/cm^2. It's demonstrated that both V_{oc} and J_{sc} has been greatly improved with the TPs. In Fig. 7(b), the figure shows that the maximum power of the "Planar" is 1.42 mW/cm^2 and the maximum power of the "TP" is 7.56 mW/cm^2. The P_{max} of "TP" has been increased more than five fold than "Planar". The ideal short-circuit current density we calculated with Eq. (6) is 50.4 mA/cm^2. However, the calculation takes into account the effect of the front surface electrode coverage and various recombination. Under non-ideal conditions, the maximum

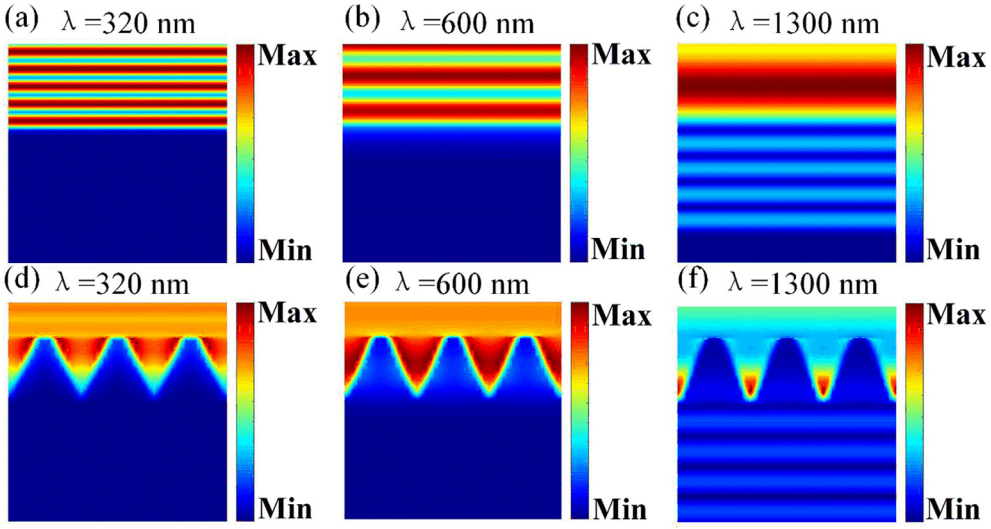

Fig. 6. The electric field intensity of HSCs without TPs at the wavelengths of 320 nm, 600 nm and 1300 nm (a–c). The Electric field intensity of HSCs with TPs at the wavelengths of 320 nm, 600 nm and 1300 nm (d–f). (The height of TPs is fixed 300 nm, the length of top and bottom side are fixed 20 nm and 80 nm respectively.)

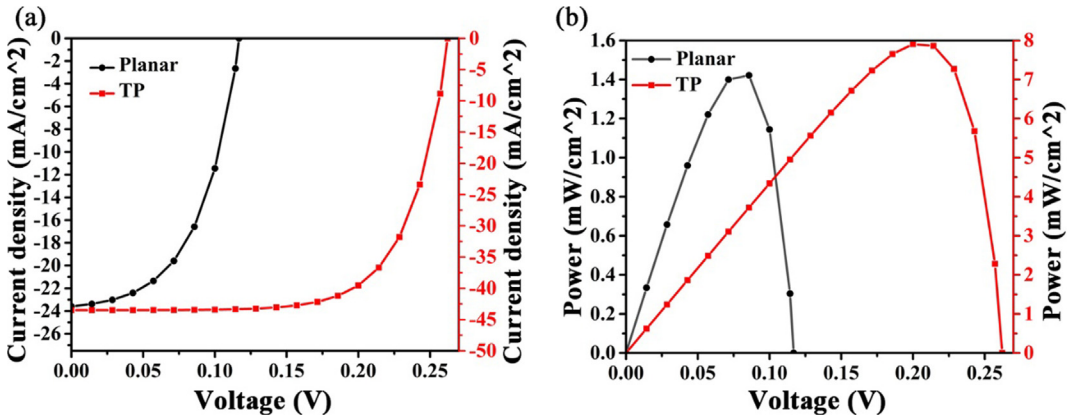

Fig. 7. (a) The J-V relationship of the HSCs with and without the TPs. (b) The P-V relationship of the HSCs with and without the TPs. (The height of TPs is fixed 300 nm, the length of top and bottom side are fixed 20 nm and 80 nm respectively.)

short-circuit current is 43.47 mA/cm^2. The open circuit voltage is the maximum voltage that a solar cell can obtain. The open circuit voltage can determine by the following expression (Onyegam et al., 2013):

$$V_{oc} = \frac{kT}{q}\ln\left(\frac{J_{sc}}{J_0} + 1\right) \tag{7}$$

where k is Boltzmann constant, T is the simulation temperature (T = 300 K), J_0 is the reverse saturation current density, it is determined by the following expression:

$$J_0 = A\exp\left(-\frac{qE_g}{kT}\right) \tag{8}$$

where A is the proportionality coefficient ($A = 1.5 \times 10^8$ mA/cm^2 (Zhou et al., 2020), E_g is the band gap of Ge at 300 K (E_g = 0.66 eV). Through Eq. (8), we can calculate the value of J_0 is 1.25×10^{-3} mA/cm^2. Then, through the Eq. (7) (J_{sc} = 43.47 mA/cm^2), we can calculate the value of V_{oc} is 0.27 V, which is slightly higher than the value of electrical simulation.

Fig. 8(a) is the J_{sc} of the trapezoid-pyramidal PEDOT:PSS/c-Ge HSCs with different pyramidal heights. It shows that the maximum J_{sc} is 43.47 mA/cm^2 at a height of 300 nm and the minimum J_{sc} is 32.46 mA/cm^2 at a height of 100 nm. It's indicated that the J_{sc} can be increased with the height of TPs. It's mainly caused by the difference capability of optical capture with different geometric parameters. Fig. 8(b) is the J_{sc} of the trapezoid-pyramidal PEDOT:PSS/c-Ge HSCs with different ratio of area (T^2/B^2). We can see that when the ratio of area is 1/16, the maximum value of J_{sc} is 42.47 mA/cm^2, and the minimum J_{sc} is 29.49 mA/cm^2 at the ratio of 1/1. The figure shows that the J_{sc} is increasing with the decrease of the ratio.

Fig. 9(a) shows the J-V curve at the height of 300 nm, 200 nm and 100 nm respectively. It shows that the maximum J_{sc} is 43.47 mA/cm^2 at the height of 300 nm. The J_{sc} is 42.15 mA/cm^2 with a height of 200 nm. The J_{sc} is 40.73 mA/cm^2 with a height of 100 nm. However, the voltage of the TPs with a height of 200 nm is slightly greater than voltage of the TPs with a height of 300 nm after about 0.21 V. Besides, the three heights show almost equivalent V_{oc}. Fig. 9(b) shows the P-V curve at the height of 300 nm, 200 nm and 100 nm respectively. From the figure, we can see that the power curve at the height of 300 nm is almost coincident to the height of 200 nm. And the power curve at the height of 100 nm is obviously lower than the others. The detailed photovoltaic parameters of different heights calculated by DEVICE are listed in Table 1.

We list the electrical performance parameters of trapezoid-pyramidal PEDOT:PSS/c-Ge HSCs with different heights above The maximum value of each parameter of the SCs has been bolded. We can see that the electrical performance is better with trapezoidal pyramids than without trapezoidal pyramids. The table shows that almost all the photovoltaic parameters have the highest value at the height of 300 nm except FF. For the J_{sc}, the highest value is 43.47 mA/cm^2. And the height of 300 nm has the maximum efficiency of 7.9%. The efficiency of HSCs is calculated by following formula (Singh and Ravindra, 2012):

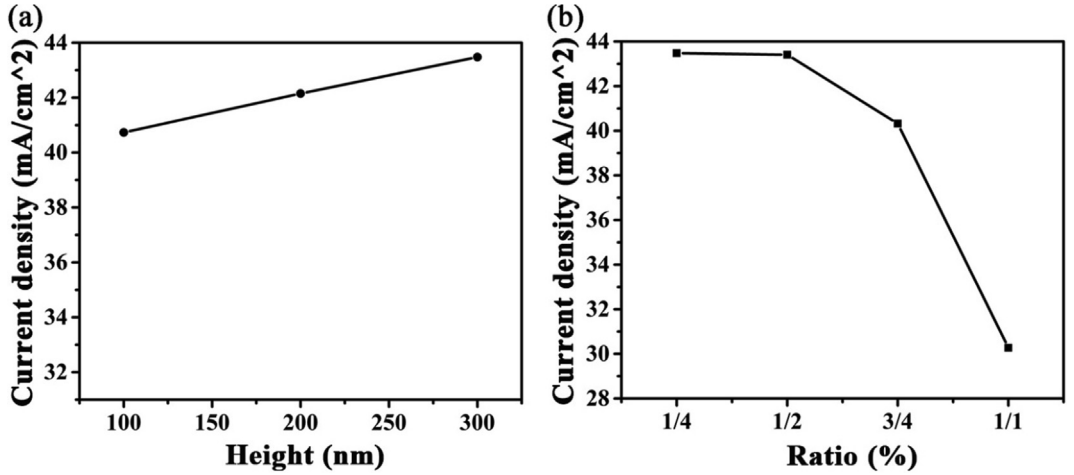

Fig. 8. (a) The J_{sc} of a trapezoid-pyramidal PEDOT:PSS/c-Ge HSCs with different pyramidal heights (h = 100 nm, 200 nm and 300 nm respectively, T^2/B^2 = 1/16). Fig. 7(b) The J_{sc} of a trapezoid-pyramidal PEDOT:PSS/c-Ge HSCs with different ratios of the length of the top and bottom side (T^2/B^2 = 1/16, 1/4, 9/16 and 1/1, the height of TPs is 300 nm).

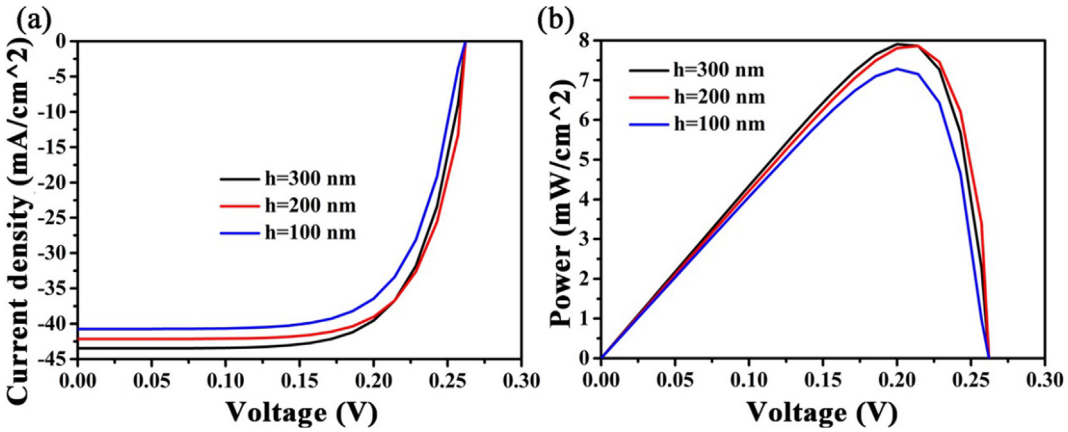

Fig. 9. (a) and (b) is the J-V and P-V curve with different heights of TPs (T^2/B^2 = 1/16).

Table 1
Photovoltaic parameters of different heights calculated by DEVICE software (h = 0 represents planar PEDOT:PSS/c-Ge HSCs).

Height (nm)	J_{sc} (mA/cm^2)	V_{oc} (V)	FF (%)	η (%)
0	23.59	0.12	52.5	1.49
100	40.37	0.25	69.0	7.28
200	42.15	0.25	70.1	7.86
300	43.47	0.26	69.3	7.90

$$\eta = \frac{P_{max}}{S_{AM1.5}} \times 100\% \tag{9}$$

where the P_{max} is the maximum power, the $S_{AM1.5}$ is the incident power from the AM 1.5 solar model and the value of $S_{AM1.5}$ is 100 mW/cm^2, so the value of P_{max} is equal to η in Table 1. Green proposed a highly accurate expression for calculating the maximum fill factor (Application Gallery, n.d.):

$$FF = \frac{\nu_{oc} - \ln(\nu_{oc} + 0.72)}{\nu_{oc} + 1} \times 100\% \tag{10}$$

where $\nu_{oc} = qV_{oc}/kT$, through the Eq. (10) (V_{oc} = 0.27 V), we can calculate the value of FF is 70.2%, this means that the fill factor should be less than 70.2%. In the electrical simulation, we did not consider the series and parallel resistance, so our fill factor is normal.

Fig. 10(a) is the J-V curve of different ratio of area, from this figure, we can see that the J_{sc} is 43.47 mA/cm^2 when the ratio of area is 1/16 while the ratio of area is 1/1 has the lowest J_{sc} of 30.27 mA/cm^2. It shows that the J_{sc} of this HSCs is inversely proportional to the ratio of area. Fig. 10(b) is the P-V curve of different ratio of area. From this figure, we can see that it's corresponding to the results of J-V curves. The P_{max} of a HSCs with a ratio of 1/16 is 7.90 mW/cm^2. The ratio of 1/1 has the lowest P_{max} of 5.29 mW/cm^2. The detailed photovoltaic parameters of different ratios calculated by DEVICE are listed in Table 2.

Table 2
Photovoltaic parameters of different ratios calculated by DEVICE software.

Ratio (%)	J_{sc} (mA/cm^2)	V_{oc} (V)	FF (%)	η (%)
1/4	43.47	0.26	69.3	7.90
1/2	43.40	0.25	68.9	7.70
3/4	40.31	0.25	68.6	7.11
1/1	30.27	0.25	68.9	5.29

We list the electrical performance parameters of trapezoid-pyramidal PEDOT:PSS/c-Ge HSCs with different ratios above. The maximum value of each parameter of the SCs has been bolded. The value of P_{max} is equal to η in Table 2. The table shows that all the photovoltaic parameters at the ratio of 1/4 have the highest value (the length of top side is 20 nm, the length of bottom side is 80 nm). It's indicated that the HSCs has more excellent photovoltaic characteristics with sharper TPs.

After changing the geometric parameters of the pyramids, it has a greater impact on the absorption of solar cell, so the short-circuit current changes greatly, but the impact on the open circuit voltage and fill factor is relatively small. By comparing the theoretical calculation with our calculated value, we can see that our calculated value is in

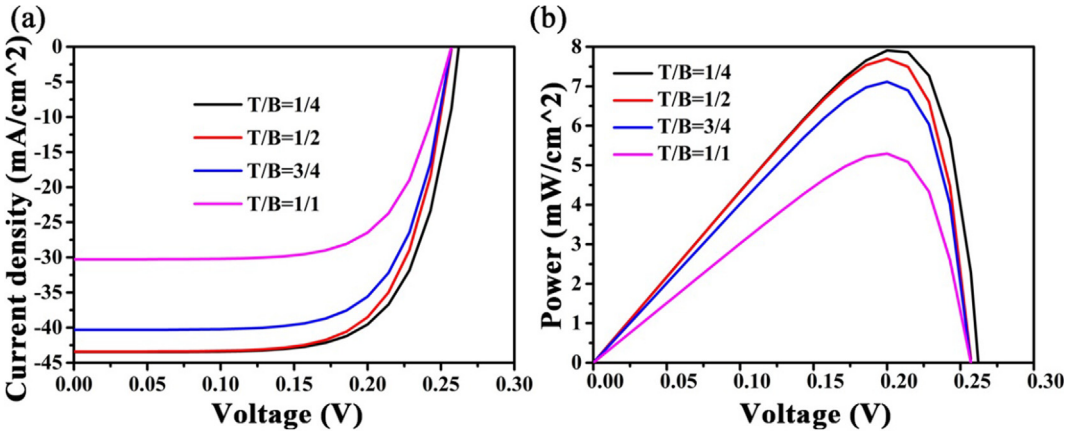

Fig. 10. (a) The J-V curve of trapezoid-pyramidal PEDOT:PSS/c-Ge HSCs with different ratios of the length of the top and bottom side. (b) The P-V curve of trapezoid-pyramidal PEDOT:PSS/c-Ge HSCs with different ratios of the length of the top and bottom side (T^2/B^2 = 1/16, 1/4, 9/16 and 1/1 respectively, the height of TPs is 300 nm).

Table 3
Comparison of solar parameters of different Ge SCs and trapezoid-pyramidal PEDOT:PSS/c-Ge HSCs.

Active layer	Thickness (μm)	FF (%)	η (%)
Ge (a-Si:H/c-Ge heterojunction SCs) (Nakano and Shiratani, 2019)	~175	61.7	7.61
Ge (a-Si:H/c-Ge heterojunction SCs) (Onyegam et al., 2013)	~50	58.1	5.28
Ge (a-Si:H/c-Ge heterojunction SCs) (Nakano et al., 2012)	~500	55.4	5.29
Ge (μc-Si:H/a-Si:H/c-Ge heterojunction SCs) (Hekmatshoar et al., 2012)	~300	62.1	7.2
Proposed (Ge (PEDOT:PSS/c-Ge HSCs))	~0.9	69.3	7.90

accordance with the theoretical calculated value. In Table 3, we compared some experiment result related to Ge solar cells studied in the past (Nakano and Shiratani, 2019; Onyegam et al., 2013; Nakano et al., 2012; Hekmatshoar et al., 2012). It can be seen from the table that our proposed solar cell is thin and efficient. Besides, due to the combination of Ge and organic PEDOT:PSS, the fill factor of SCs is effectively improved. In this table, compared with other different types of Ge solar cells, the energy conversion efficiency of our proposed solar cells is increased to 7.9%, and its fill factor is increased to 69.3%.

4. Conclusions

In conclusion, we have analyzed the optical absorption, electric field density and electrical characteristics with and without TPs. We conclude that the optical absorption of trapezoid-pyramidal PEDOT:PSS/c-Ge HSCs is basically above 90% from 300 nm to 1300 nm due to the excellent characteristic of anti-reflection. The trapezoidal pyramids structure greatly improves the absorption of solar energy by c-Ge hybrid SCs. The analysis of electric field intensity demonstrate that the great light-trapping effect because of TPs which corresponding to the result of optical absorption. The maximum J_{sc} of trapezoid-pyramidal PEDOT:PSS/c-Ge HSCs is 43.47 mA/cm^2 calculated by the DEVICE software, it is 45.73% higher than the planar PEDOT:PSS/c-Ge HSCs. In addition, the optical absorption, J_{sc}, V_{oc}, FF, P_{max} and PCE of trapezoid-pyramidal PEDOT:PSS/c-Ge HSCs with different heights and different ratios of top to bottom are compared. By theoretical calculation, HSCs composed of c-Ge and PEDOT:PSS can improve the fill factor, a HSCs with only 600 nm active layer achieves 7.9% efficiency (considering the pyramid array, the total thickness is 900 nm.).

Declaration of Competing Interest

We declare that we have no financial and personal relationships with other people or organizations that can inappropriately influence our work, there is no professional or other personal interest of any nature or kind in any product, service and/or company that could be construed as influencing the position presented in, or the review of, the manuscript entitled, “Study on the solar energy absorption for PEDOT:PSS/c-Ge trapezoid-pyramidal structure based hybrid solar cells”.

Acknowledgements

The authors are grateful to the support by National Natural Science Foundation of China (No. 51606158, 11604311, 11875228), the Undergraduate Innovation Fund Project Precision Funding by Southwest University of Science and Technology (No. JZ-19058).

Additional information

The authors declare no competing financial interests.

References

Abdelraouf, O.A., Allam, N.K., 2016. Towards nanostructured perovskite solar cells with enhanced efficiency: coupled optical and electrical modeling. Sol. Energy 137, 364–370.
Alcañiz, A., López, G., Martín, I., Jiménez, A., Datas, A., Calle, E., Ros, E., Gerling, L.G., Voz, C., Cañizo, C., Alcubilla, R., 2019. Germanium photovoltaic cells with MoOx hole-selective contacts Author links open overlay panel. Sol. Energy 181, 357–360.
Application Gallery [WWW Document], n.d. URL: https://apps.lumerical.com/solar_cells_methodology.html (accessed 9.8.19).
Baran, V., Cat, Y., Sertel, T., Ataser, T., Sonmez, N.A., Cakmak, M., Ozcelik, S., 2020. A comprehensive study on a stand-alone germanium (Ge) solar cell. J. Electron. Mater. 49 (2), 1249–1256.
Cheng, Y., Du, C., 2019. Broadband plasmonic absorber based on all silicon nanostructure resonators in visible region. Opt. Mater. 98, 109441.
Cheng, Y., Zou, H., Yang, J., Mao, X., Gong, R., 2018. Dual and broadband terahertz metamaterial absorber based on a compact resonator structure. Opt. Mater. Express. 8 (10), 3104–3114.
Dikshit, A.K., Mandal, N.C., Bose, S., Mukherjee, N., Chakrabarti, P., 2019. Optimization of back ITO layer as the sandwiched reflector for exploiting longer wavelength lights in thin and flexible (30 μm) single junction c-Si solar cells. Sol. Energy 193, 293–302.
Duan, X.L., Zhang, X.F., Zhang, Y.F., 2018. High performance organic-nanostructured silicon hybrid solar cell with modified surface structure. Nanoscale Res. Lett. 13 (1), 283.
Gao, E., Liu, Z., Li, H., Xu, H., Zhang, Z., Luo, X., Xiong, C., Liu, C., Zhang, B., Zhou, F., 2019. Dynamically tunable dual plasmon-induced transparency and absorption based on a single-layer patterned graphene metamaterial. Opt. Express 27 (10), 13884–13894.
Hao, L., Li, Q., Du, K., Xu, Z., Zhu, H., Liu, D., Cai, L., Ghosh, P., Qiu, M., 2019. An ultra-thin colored textile with simultaneous solar and passive heating abilities. Nano Energy 65, 103998.
He, Z.H., Xue, W.W., Cui, W., Li, C.J., Li, Z.X., Pu, L.H., Feng, J.J., Xiao, X.T., Wang, X.Y., Li, G., 2020. Tunable fano resonance and enhanced sensing in a simple Au/TiO_2 hybrid metasurface. Nanomaterials 10, 687.
Hekmatshoar, B., Shahrjerdi, D., Hopstaken, M., Fogel, K., Sadana, D.K., 2012. High-efficiency heterojunction solar cells on crystalline germanium substrates. Appl. Phys. Lett. 101 (3), 032102.
Huan, H., Jile, H., Tang, Y.J., Li, X., Yi, Z., Gao, X., Chen, X.F., Chen, J., Wu, P.H., 2020. Fabrication of ZnO@Ag@Ag_3PO_4 ternary heterojunction: superhydrophilic properties, antireflection and photocatalytic properties. Micromachines 11, 309.
Huang, H., Guo, Q., Feng, S., Zhang, C., Bi, Z., Xue, W., Yang, J., Song, J., Li, C., Xu, X., Tang, Z., Ma, W., Bo, Z., 2019. Noncovalently fused-ring electron acceptors with near-infrared absorption for high-performance organic solar cells. Nat. Commun. 10, 3038.
Ikeda, N., Koganezawa, T., Kajiya, D., Saitow, K.I., 2016. Performance of Si/PEDOT:PSS hybrid solar cell controlled by PEDOT:PSS film nanostructure. J. Phys. Chem. C 120 (34), 19043–19048.
Iman, G., Ali, A., Samaneh, S., 2020. Alternative buffer layers in Sb_2Se_3 thin-film solar cells to reduce open-circuit voltage offset. Sol. Energy 202, 294–303.
Jia, L.J., Fan, G.P., Zi, W., Ren, X.D., Liu, X.J., Liu, B., Liu, S.Z., 2017. Ge quantum dot enhanced hydrogenated amorphous silicon germanium solar cells on flexible stainless steel substrate. Sol. Energy 144, 635–642.
Kim, C.U., Yu, J.C., Jung, E.D., Choi, I.Y., Park, W., Lee, H., Kim, I., Lee, D.K., Hong, K.K., Song, M.H., Choi, K.J., 2019. Optimization of device design for low cost and high efficiency planar monolithic perovskite/silicon tandem solar cells. Nat. Energy 60, 213–221.
Li, J., Chen, Z., Yang, H., Yi, Z., Chen, X., Yao, W., Duan, T., Wu, P., Li, G., Yi, Y., 2020b. Tunable broadband solar energy absorber based on monolayer transition metal dichalcogenides materials using au nanocubes. Nanomaterials 10, 257.
Li, J., Chen, X., Yi, Z., Yang, H., Tang, Y., Yi, Y., Yao, W., Wang, J., Yi, Y., 2020a. Broadband solar energy absorber based on monolayer molybdenum disulfide using tungsten elliptical structures for thin film solar cells. Mater. Today Energy 16, 100390.
Li, Z., Liang, X., Li, G., Liu, H., Zhang, H., Guo, J., Chen, J., Shen, K., San, X., Yu, W., Schropp, R.E., Mai, Y., 2019. 9.2%-efficient core-shell structured antimony selenide nanorod array solar cells. Nat. Commun. 10, 125.
Li, C.C., Zhang, B., Xie, B.S., Zhao, X.B., Chen, J., 2020c. Tailored phase change behavior of $Na_2SO_4{\cdot}10H_2O$/expanded graphite composite for thermal energy storage. Energy Convers. Manage. 208, 112586.
Liu, X.J., Da, Y., Xuan, Y.M., 2017. Full-spectrum light management by pseudo-disordered moth-eye structures for thin film solar cells. Opt. Express 25 (16), A824–A839.
Liu, Z., Liu, G., Huang, Z., Liu, X., Fu, G., 2018. Ultra-broadband perfect solar absorber by an ultra-thin refractory titanium nitride meta-surface. Sol. Energy Mater. Sol. Cell. 179, 346–352.
Liu, Z., Gao, E., Zhang, Z., Li, H., Xu, H., Luo, X., Zhou, F., 2020c. Dual-mode on-to-off modulation of plasmon-induced transparency and coupling effect in patterned graphene-based terahertz metasurface. Nanoscale Res. Lett. 15 (1), 1–9.
Liu, Z., Gao, E., Zhang, X., Li, H., Xu, H., Zhang, Z., Luo, X., Zhou, F., 2020b. Terahertz

electro-optical multi-functions modulator and its coupling mechanisms based on upper-layer double graphene ribbons and lower-layer a graphene strip. New J. Phys. https://doi.org/10.1088/1367-2630/ab83d5.
Liu, G., Liu, X., Chen, J., Li, Y., Shi, L., Fu, G., Liu, Z., 2019. Near-unity, full-spectrum, nanoscale solar absorbers and near-perfect blackbody emitters. Sol. Energy Mater. Sol. Cell. 190, 20–29.
Liu, E., Tan, W., Yan, B., Xie, J., Ge, R., Liu, J., 2019. Robust transmission of orbital angular momentum mode based on a dual-cladding photonic quasi-crystal fiber. J. Phys. D Appl. Phys. 52 (32), 325110.
Liu, C., Yang, L., Liu, Q., Wang, F.M., Sun, Z.J., Sun, T., Mu, H.W., Chu, P.K., 2018. Analysis of a surface plasmon resonance probe based on photonic crystal fibers for low refractive index detection. Plasmonics 13, 779–784.
Liu, Z., Zhang, H., Fu, G., Liu, G., Liu, X., Yuan, W., Xie, Z., Tang, C., 2020a. Colloid templated semiconductor meta-surface for ultra-broadband solar energy absorber. Sol. Energy 198, 194–201.
Lumerical Support [WWW Document], n.d. URL: https://support.lumerical.com/hc/en-us/articles/360034382674-PML-boundary-conditions (accessed 9.6.19).
Lv, Y.R., Li, Y.H., Han, C., Chen, J.F., He, Z.X., Zhu, J., Dai, L., Meng, W., Wang, L., 2020. Application of porousbiomass carbon materials in vanadium redox flow battery. J. Colloid Interf. Sci. 566, 434–443.
Nakano, S., Shiratani, M., 2019. Impact of heterointerface properties of crystalline germanium heterojunction solar cells. Thin Solid Films 685, 225–233.
Nakano, S., Takeuchi, Y., Kaneko, T., Kondo, M., 2012. Influence of surface treatments on crystalline germanium heterojunction solar cell characteristics. J. Non-Cryst. Solids 358 (17), 2249–2252.
Niu, K., Sun, R.Y., Chen, Q.Y., Man, B.Y., Zhang, H.N., 2018. Passively mode-locked Er-doped fiber laser based on SnS_2 nanosheets as a saturable absorber. Photon. Res. 6, 72–76.
Onyegam, E.U., Sarkar, D., Hilali, M., Saha, S., Rao, R.A., Mathew, L., Jawarani, D., Mantey, J., Ainom, M., Garcia, R., James, W., Banerjee, S.K., 2013. Exfoliated, thin, flexible germanium heterojunction solar cell with record FF= 58.1%. Sol. Energy Mater. Sol. Cells 111, 206–211.
Orrego, S., Shoele, K., Ruas, A., Doran, K., Caggiano, B., Mittal, R., Kang, S.H., 2017. Harvesting ambient wind energy with an inverted piezoelectric flag. Appl. Energy 194, 212–222.
Pan, M., Huang, Y., Li, Q., Luo, H., Zhu, H., Kaur, S., Qiu, M., 2020. Multi-band middle-infrared-compatible camouflage with thermal management via simple photonic structures. Nano Energy 69, 104449.
Przybylski, D., Patela, S., 2019. Modelling of a two-dimensional photonic crystal as an antireflection coating for optoelectronic applications. Opto-Electron. Rev. 27 (1), 79–89.
Qi, Y.P., Zhang, Y., Liu, C.Q., Zhang, T., Zhang, B.H., Wang, L.Y., Deng, X.Y., Bai, Y.L., Wang, X.X., 2020. A tunable terahertz metamaterial absorber composed of elliptical ring graphene arrays with refractive index sensing application. Result Phys. 16, 103012.
Qin, F., Chen, X., Yi, Z., Yao, W., Yang, H., Tang, Y., Yi, Y., Li, H., Yi, Y., 2020. Ultra-broadband and wide-angle perfect solar absorber based on TiN nanodisk and Ti thin film structure. Sol. Energy Mater. Sol. Cells 211, 110535.
Qin, F., Chen, Z., Chen, X., Yi, Z., Yao, W., Duan, T., Wu, P., Yang, H., Li, G., Yi, Y., 2020. A tunable triple-band near-infrared metamaterial absorber based on au nano-cuboids array. Nanomaterials 10 (2), 207.
Ren, X., Cheng, J., Zhang, S., Li, X., Rao, T., Huo, L., Hou, J., Choy, W.C., 2016. High efficiency organic solar cells achieved by the simultaneous plasmon-optical and plasmon-electrical effects from plasmonic asymmetric modes of gold nanostars. Small 12 (37), 5200–5207.
Shi, Y., Wang, X., Liu, W., Yang, T., Ma, J., Yang, F., 2014. Nanopyramids and rear-located Ag nanoparticles for broad spectrum absorption enhancement in thin-film solar cells. Opt. Express 22 (17), 20473–20480.
Singh, P., Ravindra, N.M., 2012. Temperature dependence of solar cell performance-an analysis. Sol. Energy Mater. Sol. Cells 101, 36–45.
Sun, F., Yao, Y., Li, G., Li, X., 2018. Geothermal energy development by circulating CO_2 in a U-shaped closed loop geothermal system. Energy Convers. Manage. 174, 971–982.
Taguchi, M., Yano, A., Tohoda, S., Matsuyama, K., Nakamura, Y., Nishiwaki, T., Fujita, K., Maruyama, E., 2013. 24.7% record efficiency HIT solar cell on thin silicon wafer. IEEE J. Photovolt. 4 (1), 96–99.
Van der Heide, J., Posthuma, N.E., Flamand, G., Geens, W., Poortmans, J., 2009. Cost-efficient thermophotovoltaic cells based on germanium substrates. Sol. Energy Mater. Sol. Cells 93 (10), 1810–1816.
Wang, Y.Y., Chen, Z.Q., Xu, D.Y., Yi, Z., Chen, X.F., Chen, J., Tang, Y.J., Wu, P.H., Li, G.F., Yi, Y.G., 2020a. Triple-band perfect metamaterial absorber with good operating angle polarization tolerance based on split ring arrays. Result Phys. 16, 102951.
Wang, Y.P., Yang, H., Sun, X.F., Zhang, H.M., Xian, T., 2020c. Preparation and photo-catalytic application of ternary n-$BaTiO_3$/Ag/p-AgBr heterostructured photocatalysts for dye degradation. Mater. Res. Bull. 124, 110754.
Wang, Y.P., Jiang, F.C., Chen, J.F., Sun, X.F., Xian, T., Yang, H., 2020b. In situ construction of CNT/CuS hybrids and their application in photodegradation for removing organic dyes. Nanomaterials 10, 178.
Wang, X.X., Zhu, J.K., Wen, X.L., Wu, X.X., Wu, Y., Su, Y.W., Tong, H., Qi, Y.P., Yang, H., 2019. Wide range refractive index sensor based on a coupled structure of Au nanocubes and Au film. Opt. Mater. Express 9 (7), 3079–3088.
Wei, W.R., Tsai, M.L., Ho, S.T., Tai, S.H., Ho, C.R., Tsai, S.H., Ho, C.R., Tsai, S.H., Liu, C.W., Chung, R.J., He, J.H., 2013. Above-11%-efficiency organic–inorganic hybrid solar cells with omnidirectional harvesting characteristics by employing hierarchical photon-trapping structures. Nano Lett. 13 (8), 3658–3663.
Wu, P.H., Chen, Z.Q., Jile, H., Zhang, C.F., Xu, D.Y., Lv, L., 2020. An infrared perfect absorber based on metal-dielectric-metal multi-layer films with nanocircle holes arrays. Results Phys. 16, 102952.
Wu, H., Jile, H., Chen, Z., Xu, D., Yi, Z., Chen, X., Chen, J., Yao, W., Wu, P., Yi, Y., 2020. Fabrication of ZnO@MoS_2 nanocomposite heterojunction arrays and their photoelectric properties. Micromachines 11, 189.
Wu, P.H., Zhang, C.F., Tang, Y.J., Liu, B., Lv, L., 2020. A Perfect absorber based on similar Fabry-Perot four-band in the visible range. Nanomaterials 10, 488.
Yan, W., Tao, Z., Gu, M., Richards, B.S., 2017. Photocurrent enhancement of ultrathin front-textured crystalline silicon solar cells by rear-located periodic silver nanoarrays. Sol. Energy 150, 156–160.
Yang, W.S., Noh, J.H., Jeon, N.J., Kim, Y.C., Ryu, S., Seo, J., Seok, S.I., 2015. High-performance photovoltaic perovskite layers fabricated through intramolecular exchange. Science 348 (6240), 1234–1237.
Yi, Z., Zeng, Y., Wu, H., Chen, X., Fan, Y., Yang, H., Tang, Y., Yi, Y., Wang, J., Wu, P., 2019. Synthesis, surface properties, crystal structure and dye-sensitized solar cell performance of TiO_2 nanotube arrays anodized under different parameters. Result Phys. 15, 102609.
Yu, P., Chen, X., Yi, Z., Tang, Y., Yang, H., Zhou, Z., Duan, T., Cheng, S., Zhang, J., Yi, Y., 2019. A numerical research of wideband solar absorber based on refractory metal from visible to near infrared. Opt. Mater. 97, 109400.
Zhang, Y., Tian, F., Su, Z., Bai, R., Li, L., Yang, X., Zhang, J., 2020. Broadband single-polarization optical fiber based on surface plasmon resonance. Appl. Opt. 59 (3), 779–784.
Zhang, Y., Wu, P., Zhou, Z., Chen, X., Yi, Z., Zhu, J., Zhang, T., Jile, H., 2020. Study on temperature adjustable terahertz metamaterial absorber based on vanadium dioxide. IEEE Access. https://doi.org/10.1109/ACCESS.2020.2992700.
Zhang, X., Yang, D., Yang, Z., Guo, X., Liu, B., Ren, X., Liu, S.F., 2016. Improved PEDOT:PSS/c-Si hybrid solar cell using inverted structure and effective passivation. Sci. Rep. 6, 35091.
Zhang, G., Zhao, J., Chow, P.C., Jiang, K., Zhang, J., Zhu, Z., Zhang, J., Huang, F., Yan, H., 2018. Nonfullerene acceptor molecules for bulk heterojunction organic solar cells. Chem. Rev. 118 (7), 3447–3507.
Zhou, Z., Li, J., Xiong, Z., Cao, L., Fu, Y., Gao, Z., 2020. Reducing transition temperature and diluting brown-yellow color of VO_2 films via embedding Ag particles periodic arrays. Sol. Energy Mater. Sol. Cells 206, 110303.